a report

from the Texas A&M
RESEARCH FOUNDATION
College Station, Texas

Second

Semi-Annual Technical Report

ARPA Order Number - 1562

Grant Number - DA-ARO-D-31-124-71-G49

Program Code Number - 0D10

Principal Investigator - Dr. J. L. Stone
(713) 845-7441

Name of Grantee - Texas A&M Research Foundation

Project Scientist - (See Principal Investigator)

Effective Date of Grant - January 1, 1971

Title of Work - Characterization of Conduction Processes in Amorphous Semiconductors

Grant Expiration Date - June 30, 1972

Amount of Grant - $50,015.00

Sponsored by

Advanced Research Projects Agency
ARPA Order No. 1562

1. Introduction

This report describes work carried out during the second six month period under grant number DA-ARO-D-31-124-71-G49. Emphasis during this period was a furthering of the theory of the photodielectric effect, theoretical development for a continuous distribution of traps and its effect on the thermally stimulated conductivity, construction of experimental apparatus for the thermally stimulated conductivity tests, and the initiation of studies regarding Hall effect in insulating materials.

Early negative results associated with the observation of the photodielectric effect in amorphous semiconductors led to concentration on the thermally stimulated conductivity (TSC) for information regarding the trap distributions and concentrations. It was felt that this approach would lead to information which would shed insight into the lack of the photodielectric effect (P/D). An early literature review, however, revealed that no information was available to describe TSC in materials with continuous or quasi-continuous trap distributions. A separate section of original work is included to theoretically describe this situation.

The photodielectric effect is interpreted in terms of a short relaxation time model with experimental results suggesting relaxation between carriers over a distance equivalent to a single lattice spacing. This is not entirely surprising since the topological disorder associated with the amorphous materials strongly suggests this possibility. If the prediction is correct, it is apparent that the P/D effect will not be observed in any of the materials, since unrealistically high frequency electric fields of interaction would be required.

The measurement of the Hall effect over wide temperature ranges is complicated in amorphous materials because of the intrinsic behavior (high resistivity). A unique differential technique is discussed which will hopefully lead to more meaningful Hall data. This experiment will be considered during the remainder of the contract period.

2. Photodielectric Effect in Amorphous Materials

2-1 Introduction

The near intrinsic semiconductor behavior and observed polarization effects common to many amorphous chalcogenides suggest that the materials can be treated as lossy dielectrics. This is further enhanced by the observation that little or no impurity conduction exists in these materials. This of course does not exclude the possibility of various levels being present in the forbidden band which may have a substantial effect on the behavior of charge carriers in the material. Early papers by Kolomiets and Lyubin[1,2,3] have established the existence of recombination centers which exhibit a fast photodecay and trapping sites which display long decays in photoconductivity. More recently photoconductivity studies by Fagen and Fritzsche[4] on two chalcogenide glasses exhibiting the Ovshinsky efffect led to the formulation of a single trapping model for covalently bonded amorphous alloys. Their results indicated a continuous, rather than discrete, distribution of trapping sites within the forbidden band. They suggest that the long persistence of the photostimulated dark conductivity is caused by phonon-assisted tunneling between spatially separated localized states, a naturally slow process. Vitreous As_2S_3, the most highly resistant of the arsenic chalcogenides, has the property of a semiconductor and a dielectric[5]. The latter property is shown by the existence of high voltage polarization. The accumulation of bulk charges in photopolarization is attributed to reorientation of arsenic-sulphur chains or to electric charges being liberated by light or electric field and sticking at the ends of the chains. On the band model this would be described as due to the presence of a group of traps with energies deep in the forbidden gap, where the current carriers have small

mobilities and can be liberated only by the influence of light. Kolomiets et al.[6] have shown at least two such quasi-continuous local state groups in the ranges 1-1.3 eV and 1.5-2.3 eV in As_2S_3. It would appear that there is ample evidence of the importance of trapping dynamics in determining conduction mechanisms in amorphous semiconductors and thus is an important tool for understanding localized states.

This paper describes a unique approach to identifying the trapping sites present in the forbidden band.

2-2 The Photodielectric Effect

At low temperatures an intrinsic semiconductor can be described as a lossy dielectric. The valence band electrons are bound much less tightly than those of a good insulator thus providing the opportunity for valence band electrons or carriers in forbidden band states to participate in conduction by gaining sufficient thermal or photon energy. In well established material properties studies, Arndt, Hartwig, and Stone[7] and Hartwig and Hinds[8] have shown that the complex conductivity of semiconductors can be effectively changed by photon-induced free carrier creation. If the created carriers are allowed to react with a high frequency electric field, a phase shift in the velocity of the free carriers will result if the frequency-free carrier relaxation time product is approximately equal to or greater than unity. Such a lag in the motion of charge with respect to the field results in a complex mobility which reflects a change in both the real and imaginary parts of the complex dielectric constant of the material. The changes in the complex dielectric constant can be suitably detected by perturbation of a high frequency resonant cavity both in its resonant frequency and Q.

2-2.1 Cavity Perturbation

Sucher and Fox[9] showed that a small perturbation of a resonant cavity resulted in a change in both resonant frequency and cavity Q. Thus, the change in the complex angular frequency ω is given by

$$\frac{\delta\omega}{\omega} \approx \frac{\Delta f}{f} + j\,\frac{1}{2}\left(\frac{\Delta Q}{Q^2}\right) \qquad 2\text{-}1$$

where f is the measured resonant frequency and Q is the quality factor. A general expression for a dielectric perturbation is derived by Stone[10] as

$$\frac{\delta\omega}{\omega} = \varepsilon_0 G\left[\frac{1}{\varepsilon_2} - \frac{1}{\varepsilon_1}\right] \qquad 2\text{-}2$$

where ε_2 and ε_1 are the complex dielectric constants with and without optical and/or thermal excitation, respectively, and G is the geometric filling factor which is experimentally determined. Thus, the real part of equation 2-2 is related to the frequency change and the imaginary part is related to the Q change (see equation 2-1). Equation 2-2 is completely general and should apply to all materials if an expression for the complex dielectric constant as a function of excitation can be derived.

2-2.2 Free Carrier Effects

The classical expression for free carriers subject to a periodic field in a crystal lattice exhibiting depolarizing forces as given by Dresselhaus, Kip, and Kittel[11] and Michel and Rosenblum[12] leads to the classical complex permittivity.

$$\varepsilon^*/\varepsilon_0 = \varepsilon' - j\varepsilon''$$

$$= \varepsilon_\ell - [ne^2\tau^2(\omega_L/\omega)/m^*\varepsilon_0\varepsilon_\ell(1 + \omega_L^2\tau^2)] \qquad 2\text{-}3$$

$$- j[ne^2(\tau/\omega)/m^*\varepsilon_0\varepsilon_\ell(1 + \omega_L^2\tau^2)]$$

where ε_ℓ = lattice component, $\omega_L = \omega(1 - \omega_p^2/\omega^2)$, $\omega_p^2 = L_i(\frac{ne^2}{m^*\varepsilon_0})$, the plasma frequency, and $L_i = L/(1 + \chi L)$. For thin cylindrical wafers, $L_i = 1/\varepsilon_\ell$. The depolarizing term is a direct function of n, the density of free carriers, which can be thermally or optically induced. For convenience of interpretation of data, the experiment is run at low temperature to suppress the thermal contribution.

Since the above treatment is derived only for a free carrier contribution, additional terms must be considered to explain trapping effects.

2-2.3 Trapping Effects

Hartwig and Hinds[8] have considered the photodielectric effect in CdS for which trapping dynamics play the dominant role. The authors assume a classical harmonic oscillator model for trapped carriers which are considered to be polarizable centers. With these assumptions they find

$$\Delta\varepsilon = \frac{ne^2}{m^*\varepsilon_0}\left[\frac{\omega_0^2 - \omega^2 - j\omega/\tau}{(\omega_0^2 - \omega^2)^2 + (\omega/\tau)^2}\right] \qquad 2\text{-}4$$

Here ω_0 is the frequency of the classical oscillator. The frequency of the oscillator is proportional to E^3, where E is the binding energy for the particular trap. It is found that deep traps are less polarizable than shallow ones and normally can be neglected in the photodielectric effect.

If the lifetime of the carriers in traps is long, the effective change in frequency due to the change in the real part of the dielectric constant will represent an integration of the number of created polarizable centers.

2-2.4 Traps in Amorphous Semiconductors

In the previous section it is pointed out that the photodielectric effect has been exhibited due to the presence of polarizable traps. Since models have been suggested which place many trapping sites in the forbidden band of amorphous semiconductors, the photodielectric effect would appear to be a sensitive test for providing detailed information about the trapping dynamics.

Cohen[13] has applied the effects of trapping sites to the CFO model for amorphous materials. Andriesh and Kolomiets[14] report the presence of current carrier trapping centers in the forbidden band of the amorphous semiconductor $Tl_2Se \cdot As_2Te_3$. Also multiple trapping levels are reported in the amorphous chalcogenide alloy As(50%)-Te(30%)-Ge(11%)-Si(9%) by Botila and Vancu[15]. Kolomiets, Lyubin, and Averjanov[16] describe the existence of both trapping sites and recombination centers in As_2Se_3.

The theoretical model for the complex dielectric constant change for an amorphous semiconductor has not been treated in the literature. It is uncertain whether either the free carrier of trapping model which have been used successfully in other materials are suitable for the amorphous state. However, regardless of the process involved, the general expression of equation 2-2 should hold.

2-3 Experimental Techniques

Several different samples of $2As_2Se_3 \cdot As_2Te_3$, As_2Se_3, As_2Te_3, As_2S_3, and Si(3%)-Ge(4%)-As(38%)-Te(55%) were fabricated using standard

techniques. The materials were found to be amorphous in bulk form as verified. by X-ray diffraction studies and electron microscopy.

2-3.1 Microwave Equipment

A TE-011 cylindrical cavity is used to house the test sample. Coupling to the reflection cavity is magnetic and the sample is held in a position of maximum electric field by a teflon support. The sample is photon excited by light of variable wavelength entering through a small hole in the cavity wall, as shown in Figure 2-1. The resonant frequency of the loaded cavity was 11.87 GHz. The use of an oscillator synchronizer allowed frequency changes of approximately 1 part in 10^8 to be resolved. The loaded Q of the cavity was measured with and without the sample and it was confirmed that the sample dominated the loaded Q. Therefore, dielectric changes in the sample reflect directly as frequency and Q changes of the cavity. The microwave arrangement is shown in Figure 2-2.

2-3.2 Cryogenic Equipment

A standard two piece dewar set was used to allow measurements to be conveniently made at liquid helium, liquid nitrogen, or room temperatures. Optical flats in the two dewars were used to bring light into the cryogenically cooled cavity and sample. This is shown in Figure 2-3.

2-3.3 Optical Excitation

A He-Ne gas laser, Electro Optics LAS-2002 was used to provide photon energy of approximately 1.965 eV. Long wavelength excitation was obtained from a high intensity projector lamp and a mercury arc lamp containing lines from 1850Å to 5361Å was used for excitation near 6.5 eV. Some dispersion caused by the liquefied gases was experienced.

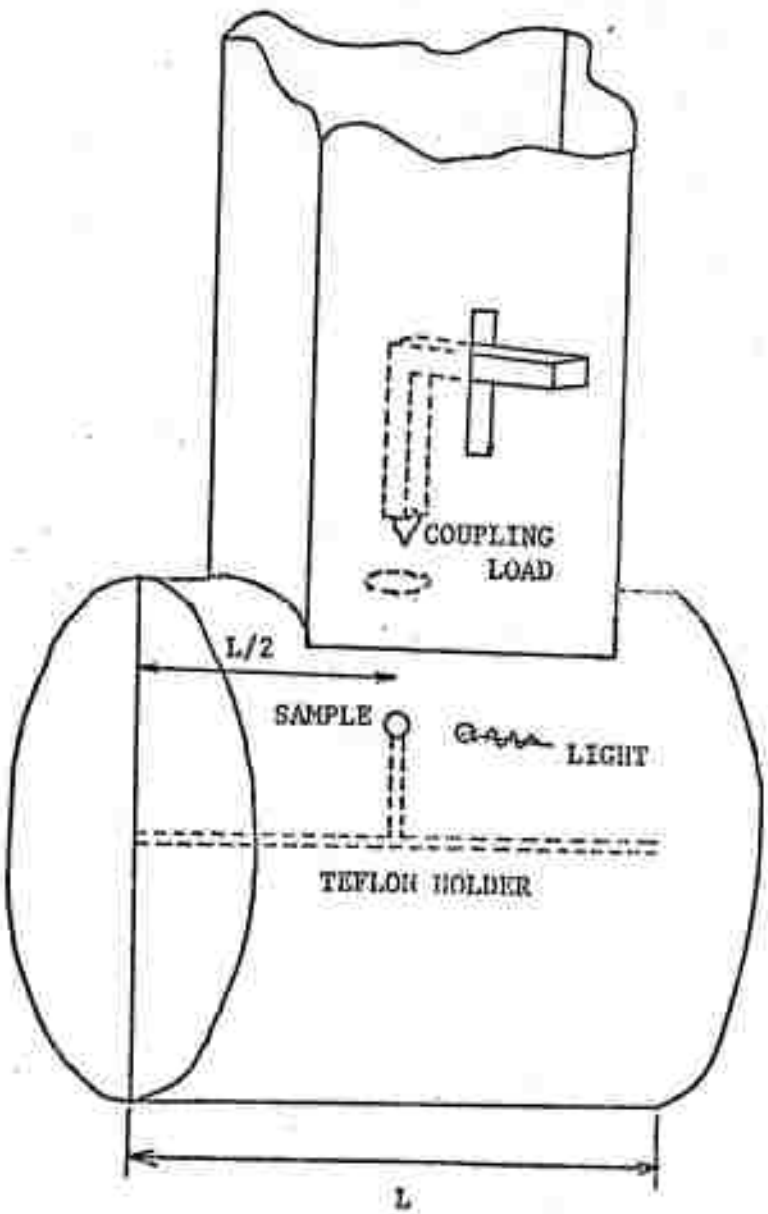

Figure 2-1. Cavity-Waveguide Configuration

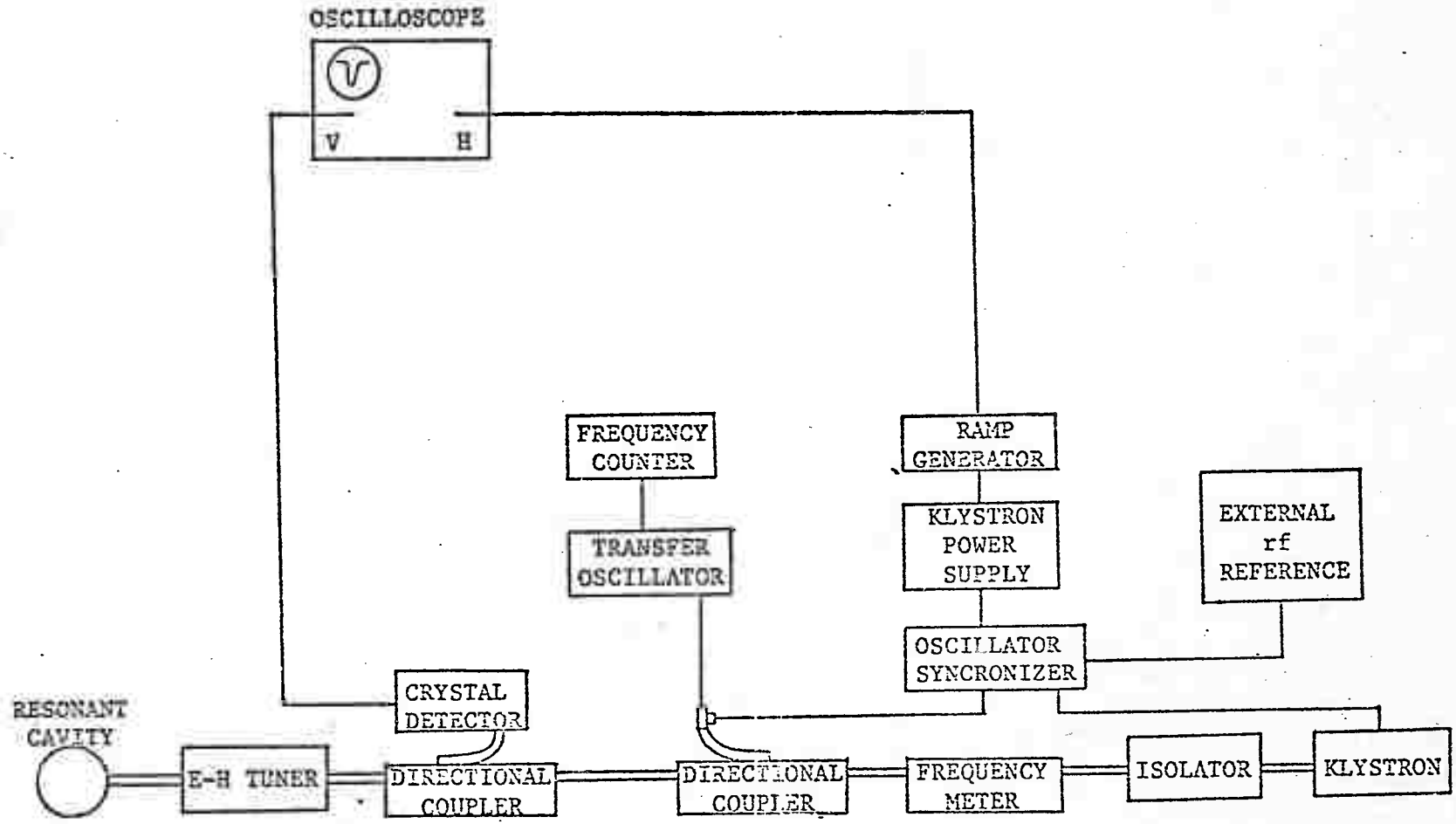

Figure 2-2. Microwave System

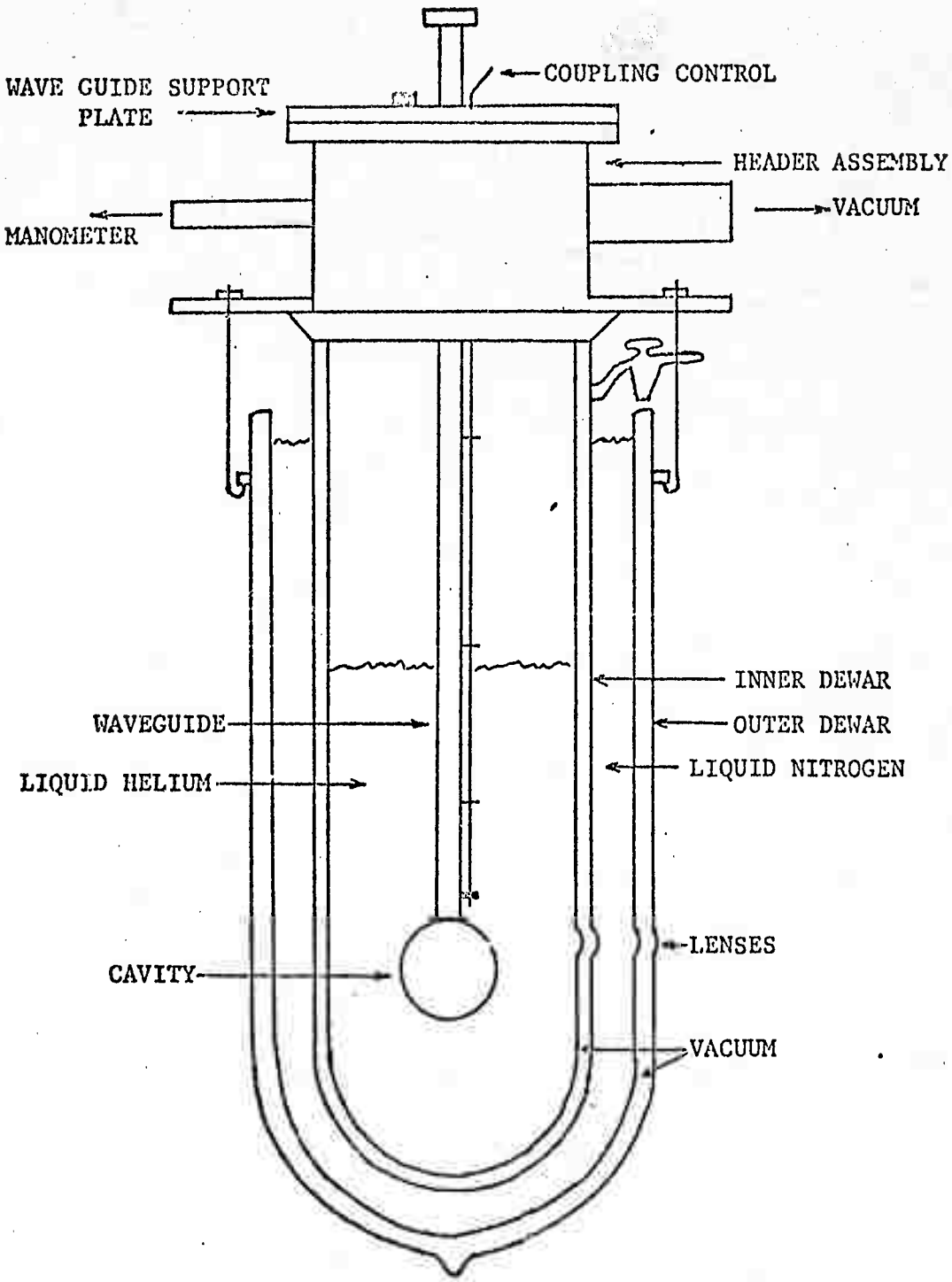

Figure 2-3. Dewar System

2-4 Experimental Results

Several different samples of $2As_2Se_3 \cdot As_2Te_3$, As_2Se_3, As_2Te_3, As_2S_3 and Si(3%)-Ge(4%)-As(38%)-Te(55%) were used in the photodielectric tests. These varied in size from about 0.3 cm in diameter and 0.1 cm thick to 0.75 cm in diameter and 0.3 cm thick. The G factors of these samples ranged from 0.00176 to 0.015. The experiment, as described in the previous section, was performed on these samples at room temperature, liquid nitrogen temperature (77°K) and liquid helium temperature (4.2°K), however, no photodielectric effect was observed.

In order to establish that the apparatus was not at fault, an Al doped sample of CdS, known to exhibit the photodielectric effect at 900 MHz, was tested. The equipment performed properly and a frequency shift of 1.61 MHz was observed in the resonant frequency of 11.9 GHz, for full illumination from the HeNe laser.

Although only negative results were obtained for the five amorphous materials tested, it is premature to postulate the lack of a photodielectric effect to be a universal feature of disordered materials. However, it is appropriate to investigate known material properties of the amorphous chalcogenides to determine if some common denominator exists that would explain the apparent lack of depolarization.

2-4.1 Density of States

Although sufficiently energetic photons were provided for band to band transitions or localized state to band transitions, there is uncertainty as to the number of created polarizable centers. In particular, if the available states in the forbidden band are considered, optical absorption data[17] predicts an upper limit of $10^{16} eV^{-1} cm^{-3}$ gap states. However, contradictory electrical data[17] sets the density of gap states at

$10^{19} eV^{-1} cm^{-3}$ in order to explain the lack of a field effect in several chalcogenides[17]. If the worst case condition is chosen, the density of states would be marginal for observation of polarization changes based on sensitivity predictions for the apparatus used by Hartwig and Hinds[8]. In addition, if the majority of the trapping sites are located deep in the forbidden band, Hartwig and Hinds show that the contributions to depolarization are small since the more tightly bound traps can provide smaller orbital changes and, thus, effect depolarization to a lesser extent.

Another possibility exists if the photon density is too low. If all created free carriers were used to fill the deep traps without ever saturating the less polarizable centers, then there would be no observable photodielectric effect nor would there be a Q change since there would be no conduction current to change the losses in the material. Because there is no charge injected in this electrodeless experiment, the contradictory observation of photoconductivity (with carrier injection) in the materials without a corresponding Q change when the material is in the cavity, is possibly explained. Before these suppositions can be proved or disproved, detailed thermally stimulated conductivity experiments will have to be performed to determine the trapping dynamics which are present.

2-4.2 Momentum Relaxation Time

Equations (2-3) and (2-4) show the importance of the carrier momentum relaxation time in determining the magnitude of the depolarization when the process is due to free carriers or trapping. Stone[7] has shown that the excitation frequency-relaxation time product must be greater than or approximately equal to unity for sufficient interactions of the created charge (free or bound) with the applied field. If $\omega\tau \ll 1$, then little or no

photodielectric effect is observed. For an excitation of $\omega = 2\pi\ (11.8)10^{3}$, $\tau \leq 10^{-11}$ sec. would be sufficient to negate the photodielectric effect. Such a range of relaxation times in disordered materials is certainly possible since values of 10^{-12} sec. for intrinsic crystalline silicon at room temperatures are typical. Furthermore, the absence of an electron spin resonance signal (sensitivity of $10^{17} cm^{-3}$) from chalcogenide films is attributed, by Fritzsche[17], to a short relaxation time, although no values are quoted.

The experiment at liquid helium temperature showed no photodielectric effect, thus, the upper bound on τ can be increased several orders of magnitude since τ should increase with decreasing temperature. It is interesting to consider the possibility of relaxation on the order of one lattice spacing which lead to relaxation times on the order of 10^{-15} sec.[18].

Figures 2-4, 2-5, and 2-6 show the effect of changing the momentum relaxation time for a cavity of resonant frequency 10^{9} Hz. The effect at X-Band can be obtained by extrapolation since the effect of raising frequency is very nearly linear as far as the photodielectric response is concerned. The d/b ratio is simply a loading factor which will not be used other than to compare from one curve to the others. The overall effect is seen to be the decrease in photodielectric response (y-axis) as the relaxation time is decreased. The x-axis represents light power impinging on the sample.

2-5 Conclusions

Further tests will be run when sufficient TSC data is available to confirm the trap structures present in the materials.

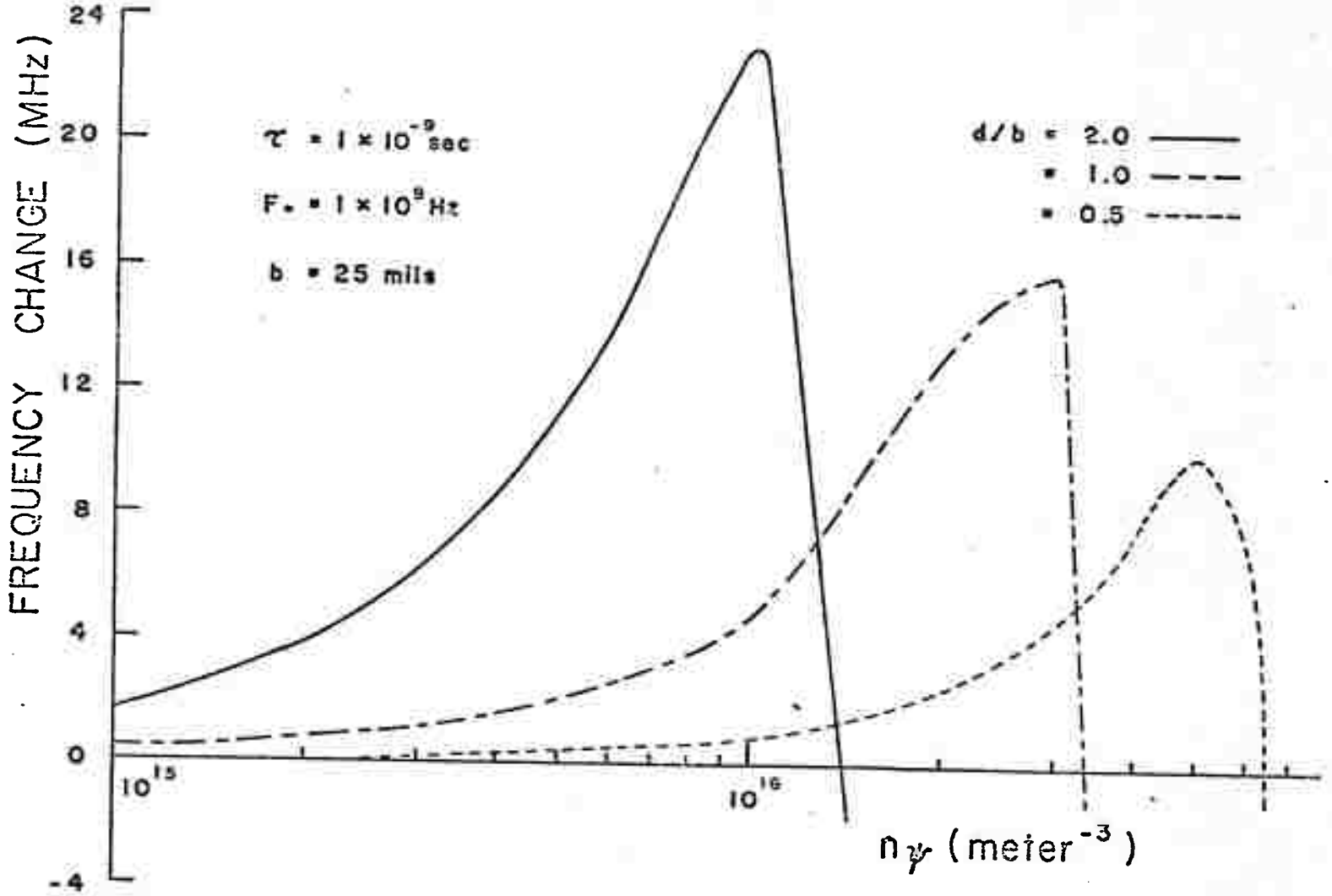

Figure 2-4. Effect of d/b Ratio, $\tau = 1 \times 10^{-9}$ sec

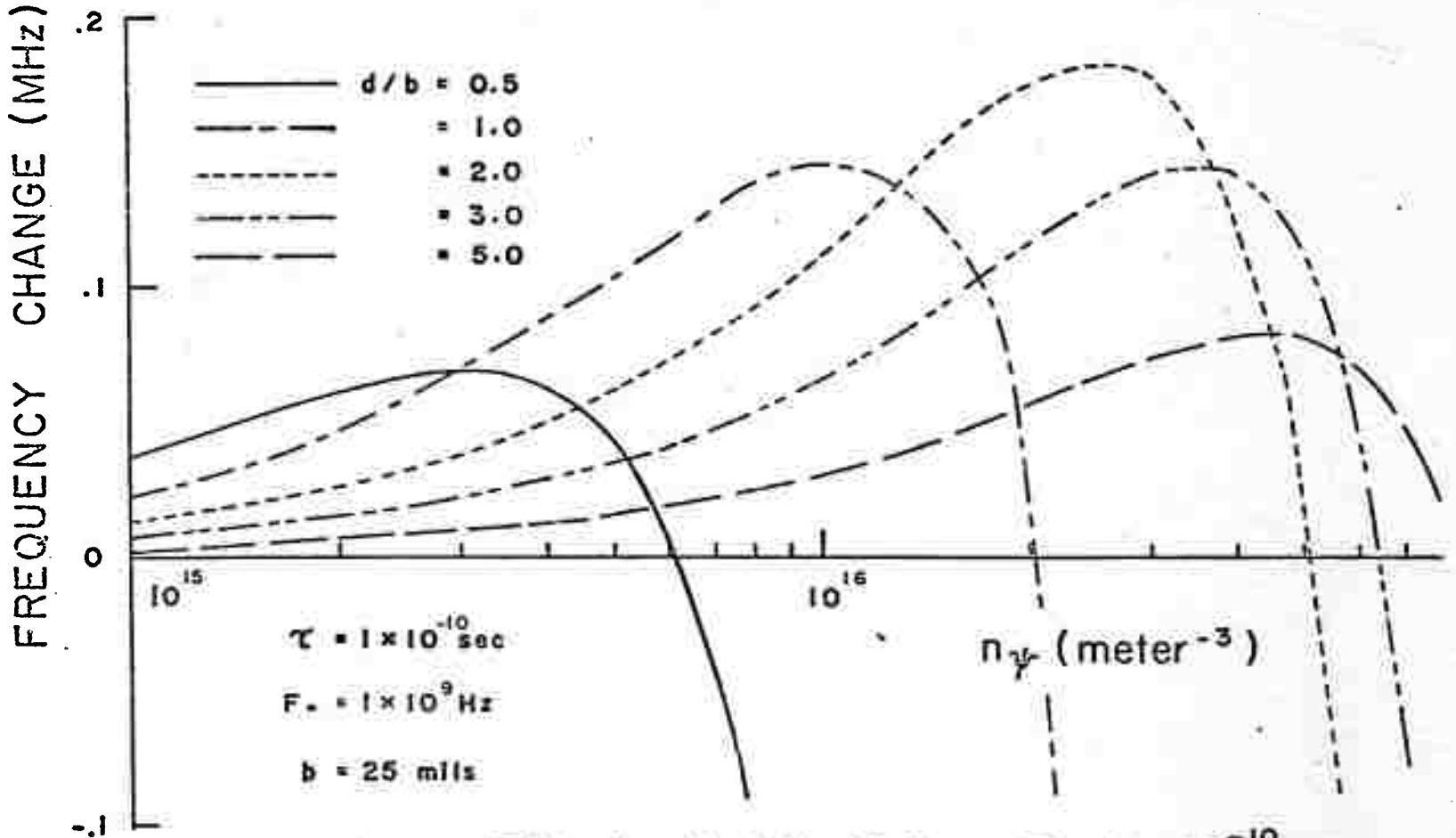

Figure 2-5. Effect of d/b Ratio, $\tau = 1 \times 10^{-10}$ sec

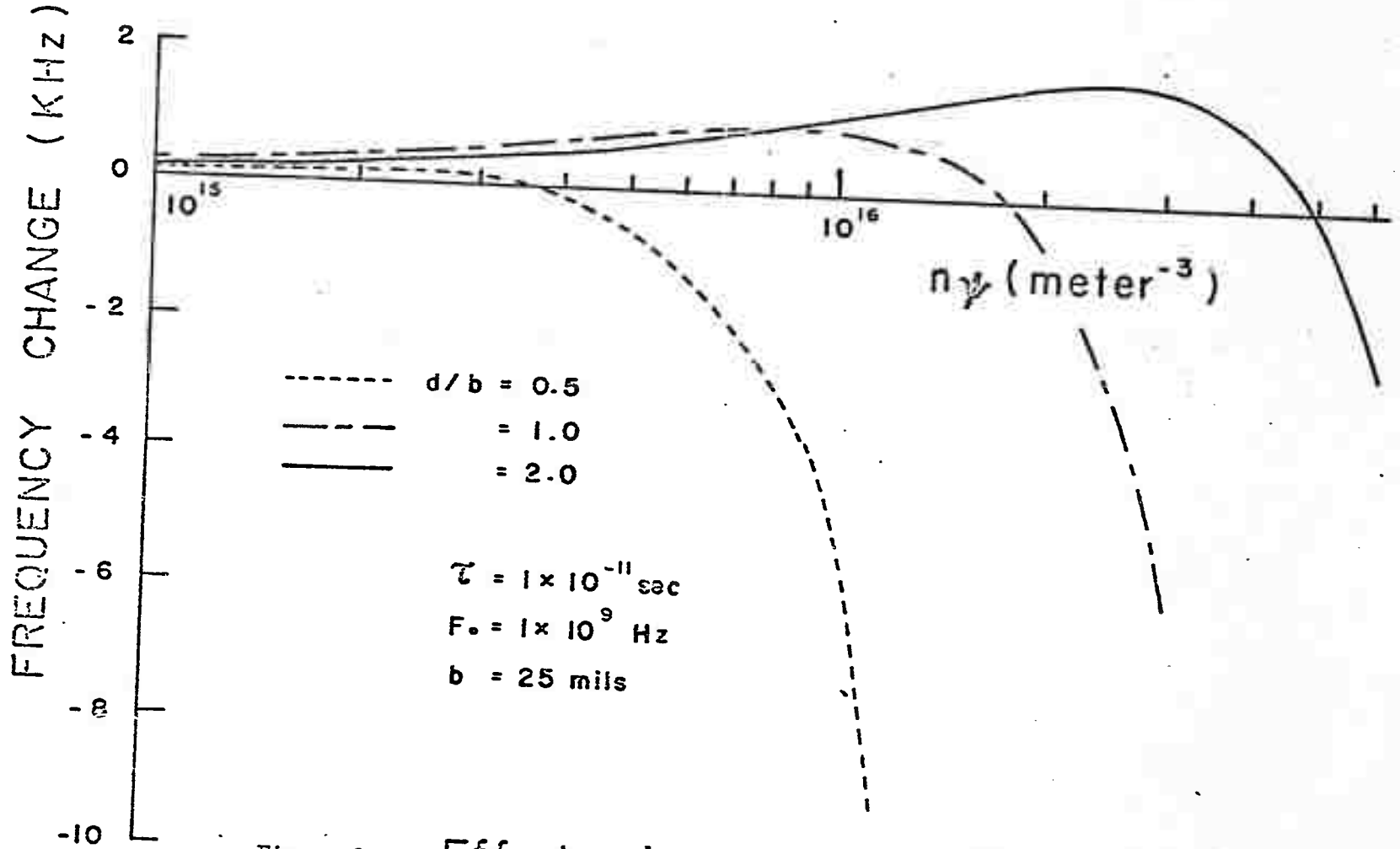

Figure 2-6. Effect of d/b Ratio, $\tau = 1 \times 10^{-11}$ sec

3. Thermally Stimulated Conductivity (TSC)

3.1 Introduction

TSC has been used quite successfully to determine the properties of traps in many of the common semiconductors. Very briefly, the specimen is normally formed into a geometry which allows parallel plane contacts to be attached to which a biasing voltage is applied. The contacts are made injecting as far as the majority carriers are concerned. The material is then cooled to liquid nitrogen (77°K) or lower with care taken that no light impinges on the specimen. The semiconductor is then exposed to light of sufficient photon energy to assure population of the conduction band. The generated free carriers instead of dropping back to the valence band (majority carriers assumed to be electrons) are captured by traps present in the lattice. These trapped carriers are essentially frozen in at all levels except for the shallowest lying states because of the low temperature. An equilibrium condition is reached when the photocurrent becomes constant. The biased crystal is then heated at a uniform rate and the temperature and current are recorded. The free carrier density can be found, of course, after the mobility is determined. Current peaks are observed as various trapping centers are emptied. (Note: all of the analysis to follow will be based on discrete levels of trapping sites. Later a derivation for continuous distributions will be presented.) As the traps begin to empty the current will increase. As the trapping level is depleted the rate of rise of the current increase will decrease, both due to retrapping and decrease of occupancy. Eventually a maximum will be reached, the current will decrease until it again follows the increase due to thermal excitation from band to band. Several peaks may be apparent indicating the presence of multiple levels.

A detailed literature search reveals various forms of analysis of the TSC curves. Particular reference is made to papers by Garlick and Gibson[19], Bube[20], Horganstraaten[21], Haering and Adams[22], Keating[23], Halperin and Braner[24], Grossweiner[25], Luschik[26], and Haine and Carley-Reed[27]. Nicholas and Words[28], Dittfeld and Voigt[29], and Bube[30] compare various methods of analysis to their data to determine the reliability and accuracy of each of the methods. However, none of these papers considers both retrapping and recombination effects simultaneously. A recent paper by Dussel and Bube[31] has considered the problem in a most general way. Their results are, however, much too complicated to be of practical value. The paper by Haine and Carley-Reed represents a compromise between simplicity and completeness.

3-2 Analysis of Discrete Trapping Levels

Three rate processes are important in analysing the TSC curves. These are rate of release of electrons from trapping levels, rate of retrapping of electrons, and the rate of recombination. These rates can be combined into a general equation

$$\frac{dn_c}{dt} = \frac{n_t \theta}{\tau_t} - \frac{n_c}{\tau_t}\left(1 - \frac{n_t}{N_t}\right) - \frac{n_c}{\tau} \qquad 3\text{-}1$$

where n_c = density of electrons in the conduction band

n_t = density of electrons in the trapping level

N_t = density of trapping centers

θ = trapping factor

τ_t = trapping time

τ = recombination lifetime.

If dn_c/dt is neglected, equation 3-1 can be solved for n_c and then differentiated with respect to temperature. If the trapping level E_t is much greater than kT, the temperature dependence of N_c (the effective density of states) can be neglected. Using this assumption and the definition

$$\Theta = (N_c/N_t) \exp(-E_t/kT) \qquad 3\text{-}2$$

an equation describing the slope at any point on the TSC curve can be derived and is given as

$$N_t(\tau + \tau_t) = \frac{\{n_c + N_c \exp(-E_t/kT)\}^2}{\dot{T} N_c \{E_t/kT^2 - n_c^1/n_c\} \exp(-E_t/kT)} \qquad 3\text{-}3$$

at a current maximum, $n_c^1 = 0$ and equation 3-3 becomes

$$N_t(\tau + \tau_t) = \frac{kT^2 N_c}{E_t \dot{T}} \exp\left(-\frac{E_t}{kT}\right) \left\{1 + \frac{n_c}{N_c} \exp\left(\frac{E_t}{kT}\right)\right\}^2 \qquad 3\text{-}4$$

If two different values of $\dot{T}$ (i.e. heating rates) are used and points of maximum current are taken from the two curves, E_t can be evaluated directly. Also $N_t(\tau + \tau_t)$ can be calculated which then requires knowledge of the characteristic times in order to determine N_t alone.

Since it appears that the trap distribution should be more or less continuous, the derivation must be extended. This is done in the next section.

3-3 Analysis of Continuously Distributed Trapping Levels

This section is divided into two parts. The first part is a qualitative description of the Thermally Stimulated Conductivity (TSC) experiment for a simplified crystal structure. The second part extends the analysis of TSC data to the generalized situation of a continuous distribution of traps in the forbidden gap.

3-3.1 Qualitative Description of TSC Experiment

In the following discussion, assume that the experiment is done on a crystal with one trapping level (at E_t) in the band gap as shown in Figure 3-1A.

At room temperature a finite number of carriers will be present in the conduction band. If the crystal is cooled, part of these carriers will lose thermal energy and fall down into the valence band. At very low temperatures (below liquid nitrogen temperature) essentially all of the carriers will be in the valence band.

If energy is pumped into the crystal while maintaining the low temperature (for example, by a light source) carriers will be excited out of the valence band to the conduction band or to a trap. However, those which reach the conduction band to not have enough thermal energy to remain there and fall back to a trap or the valence band as shown in Figure 3-1B. If this process is continued long enough, the traps will eventually become saturated.

If the crystal is then heated at some rate, the electrons in the traps will begin to gain thermal energy and will be excited to the conduction band as shown in Figure 3-1C. These electrons will cause the conductivity to increase over its normal value. As the traps empty, this increase

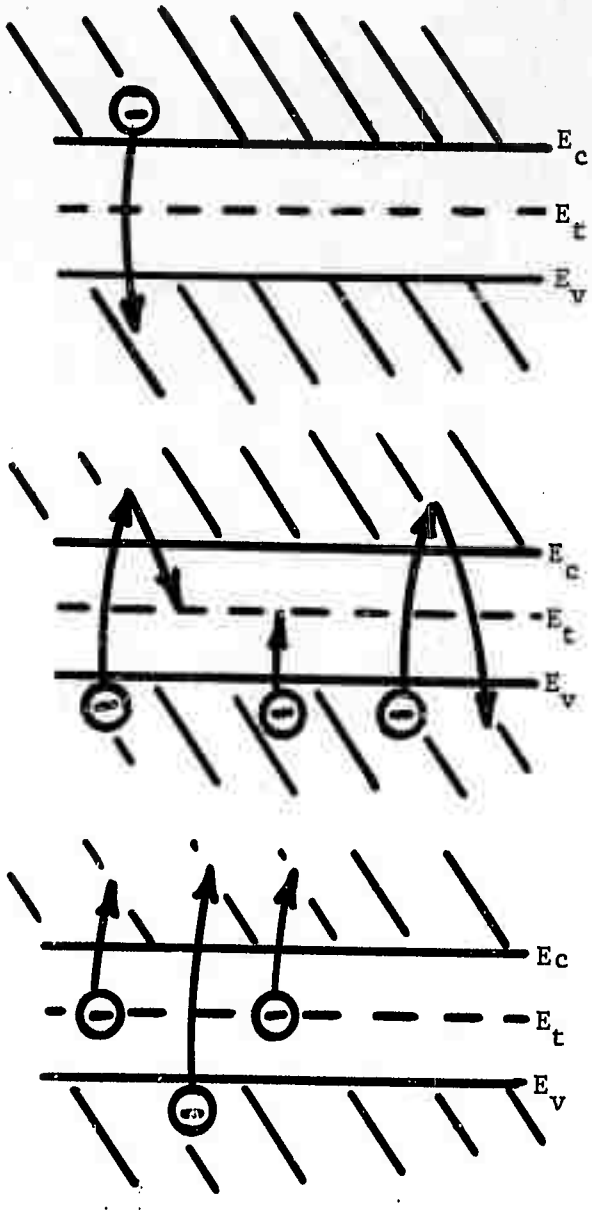

(Fig. 3-1A)

(Fig. 3-1B)

(Fig. 3-1C)

Figure 3-1: Band diagram of a crystal with one trapping level at E_t

in conductivity will reach a maximum and begin to decrease back to the normal value. By analyzing the change in conductivity, information can be obtained about the traps such as their energy depth and their density.

In amorphous materials, the situation is complicated by the fact that the forbidden gap no longer exists as such. In its place is a continuous distribution of states with low mobilities (i.e. traps[32]). The density of traps is now a continuous function of energy instead of a discrete distribution.

3-3.2 Extension of the Analysis of TSC Data

It is assumed that electrons move from traps only to conduction band. There are 3 important processes for the analysis.

(1) Rate of release of electrons from traps (R_R)

$$R_R = \frac{n_t \Theta}{\tau_t} \qquad \Theta = \frac{N_c}{N_T} \epsilon^{-E/kT} \qquad 3\text{-}5$$

where: τ_t = trapping time for an electron by trapping level with zero occupancy.

$n_t = n_t(E)$ = density of electrons at trap level E.

N_c = equivalent density of states at the bottom of the conduction band.

$N_t = N_t(E)$ = density of traps at E.

E = energy depth below E_c.

K = Boltzman's constant.

T = absolute temperature.

(2) Rate of retrapping of electrons (R_T)

$$R_T = \frac{n_c(1 - f(E))}{\tau_t} \qquad 3\text{-}6$$

where: $n_c = n_c(E)$ = density of electrons in conduction band.

$f(E)$ = Fermi function.

(3) Rate of Recombination (R_c)

$$R_c = \frac{n_c}{\tau} \qquad 3\text{-}7$$

where: τ = recombination lifetime.

These processes are related by:

$$\frac{dR_c}{dt} = R_R - R_T - R_c = \frac{n_t\theta}{\tau_t} - \frac{n_c}{\tau_t}(1 - f(E)) - \frac{n_c}{\tau} \qquad 3\text{-}8$$

It is now assumed that dn_c/dt can be neglected on the grounds that the experimental rate of change of n_c is very small compared with the relaxation time of n_c (smallest of τ or τ_t) after a perturbation in the flow processes.[32]

$$\Rightarrow \quad \frac{n_t\theta}{\tau_t} = \frac{n_c}{\tau_t}(1 - f(E)) + \frac{n_c}{\tau}$$

or

$$n_c = \frac{n_t\theta}{1 + \tau_t/\tau - f(E)} \qquad 3\text{-}9$$

taking differentials:

$$dn_c = \frac{\theta dn_t + n_t d\theta}{1 + \tau_t/\tau - f(E)} + \frac{n_t\theta df(E)}{[1 + \tau_t/\tau - f(E)]^2} \qquad 3\text{-}10$$

(Assuming that τ_t and τ are constant)

But,

$$\theta = \frac{N_c}{N_T} e^{-E/KT} \quad \Rightarrow \quad d\theta = -\frac{\theta dE}{KT} - \frac{\theta}{N_T} \frac{dN_T dE\ (F)}{dE} \qquad 3\text{-}11$$

(the temperature dependence of N_c is neglected)

and,

$$f(E) = \frac{dn_t}{dN_T} \approx e^{-E/KT} \qquad \text{(Boltzman's approximation)} \qquad 3\text{-}12$$

$$\Rightarrow \quad df(E) = -\frac{f(E)\,dE}{KT} \qquad 3\text{-}13$$

Define:

$$g(E) = \frac{dN_T}{dE} \qquad 3\text{-}14$$

Substituting 3-11, 3-12, 3-13, and 3-14 into 3-10 gives:

$$\frac{dn_c}{dE} = \frac{\theta[f(E)g(E) - n_{t/KT} - \frac{n_t}{N_T} g(E)]}{1 + \tau_t/\tau - f(E)} - \frac{n_t \theta f(E)/KT}{[1 + \tau_t/\tau - f(E)]^2} \qquad 3\text{-}15$$

Equation 3-9 gives:

$$n_t = \frac{n_c[1 + \tau_t/\tau - f(E)]}{\theta} \qquad 3\text{-}16$$

Substituting 3-16, combining, and simplifying gives:

$$\frac{dn_c}{dE} = g(E)\left[\frac{\theta f(E)}{1 + \tau_t/\tau - f(E)} - \frac{n_c}{N_T}\right] - \frac{n_c[1 + \tau_t/\tau]}{KT[1 + \tau_t/\tau - f(E)]} \qquad 3\text{-}17$$

From Equation 3-5

$$\theta = \frac{N_c}{N_T} e^{-E/KT}$$

$$\Rightarrow \quad g(E)\left[\frac{N_c e^{-E/KT} f(E)}{1 + \tau_t/\tau - f(E)} - n_c\right] - N_T\left[\frac{n_c[1 + \tau_t/\tau]}{KT[1 + \tau_t/\tau - f(E)]} - \frac{dn_c}{dE}\right] = 0 \qquad 3\text{-}18$$

Let:

$$A(E) = \left[\frac{N_c e^{-E/KT} f(E)}{1 + \tau_t/\tau - f(E)} - n_c\right] \qquad 3\text{-}19$$

and

$$B(E) = \left[\frac{n_c[1 + \tau_t/\tau]}{KT[1 + \tau_t/\tau - f(E)]} - \frac{dn_c}{dE}\right]$$

And: $$g(E) = \frac{dN_t}{dE} \qquad 3\text{-}20$$

$$\therefore \quad A(E)\frac{dN_T}{dE} - B(E)N_T = 0$$

or

$$\frac{dN_T}{dE} - \frac{B(E)}{A(E)} N_t = 0 \qquad 3\text{-}21$$

Assume that equilibrium is effectively maintained between the traps and the conduction band during the experiment.

then:

$$E = KT \ln\left(\frac{N_c}{n_c}\right) = CT \qquad 3\text{-}22$$

(Note: See Reference 32), P. 294)

Making the above change of variables in Equation 3-21 gives:

$$\frac{dN_T}{dT} - \frac{\left[C - \frac{KT}{n_c}\frac{dn_c}{dT}\right] B(CT)}{A(CT)} N_T = 0 \qquad 3\text{-}23$$

Let:

$$H(T) = \frac{\left[C - \frac{KT}{n_c}\frac{dn_c}{dT}\right] B(CT)}{A(CT)} N_t = 0 \qquad 3\text{-}24$$

$$\Rightarrow \frac{dN_T}{dT} - H(T)\, N_T = 0 \qquad 3\text{-}25$$

$$\Rightarrow N_T = \text{Exp}\left[\int_0^T H(T)\,dt\right] \qquad 3\text{-}26$$

A computer solution to equation 3-26 is being written which will be used to analyze the TSC data.

3-4 Experimental Apparatus for TSC Experiments

This section describes the design of the experimental apparatus required for conducting TSC measurements on amorphous thin film devices. A simple extension of the apparatus allows measurements to be made on bulk samples. A block diagram of the system is shown in Figure 3-2. Three main divisions of the system require special attention, namely the device holder, sample heater, and data recorder. These will be discussed separately in the following sections of the report.

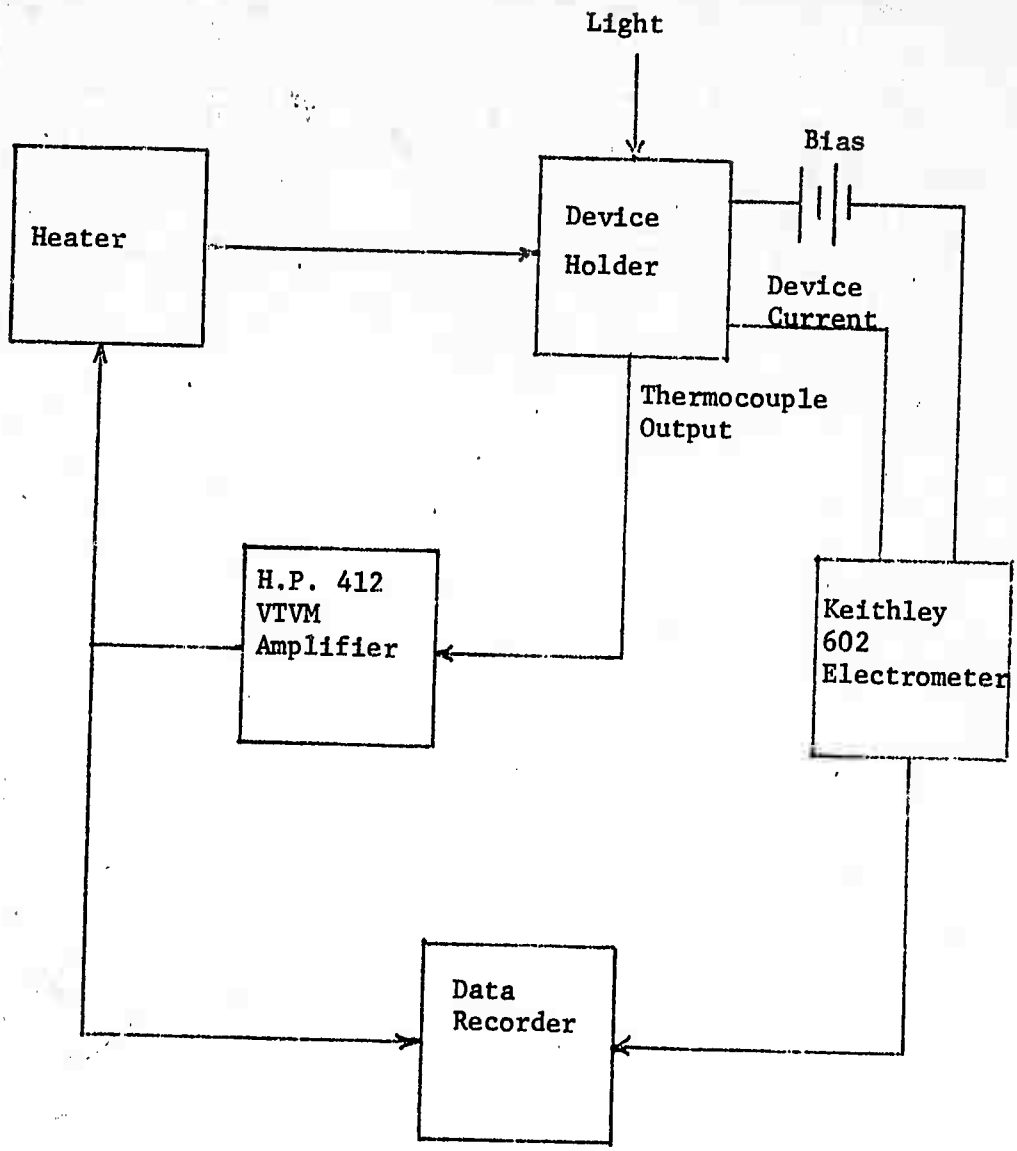

Figure 3-2: Block Diagram of the TSC System Design.

3-4.1 Sample Holder

The design of the sample holder was determined by the choice of device geometry. Several alternatives were considered and the structure shown in Figure 3-3 was chosen. A thin aluminum side-by-side contact is deposited on a glass substrate. The amorphous material is then deposited between the two contacts. The spacing can be varied and carefully controlled for repeatability by using standard mask-photo resist techniques. This geometry was considered to be most useful since the TSC measurements can be correlated with field-effect measurements on devices of similar structure.

Certain physical restraints dictated the remainder of the holder design. Most important being the following:

1. Size determined by Dewar system.
2. Temperature monitor required.
3. Sample heating required.
4. A controlled light source had to be available to the sample.
5. Necessary leads had to provide required signals with minimum heat load on the cryogenic environment.

A drawing of the final design is shown in Figure 3-4 which is not shown to scale.

The temperature monitor is a chromel-constantan thermocouple which was chosen for its high output voltage over the temperature range of interest. See Figure 3-5. The heater comprises four, 47 Ω, 2 watt, composite resistors connected in parallel. The light source required to saturate the trapping levels is an incandescent bulb. The light is taken into the Dewar by a fiber optics bundle. Leads are fastened to the aluminum contacts with an ultrasonic bonder and fine copper wire provides the signals to the ambient. The entire holder was fabricated from a simple piece of brass bar stock.

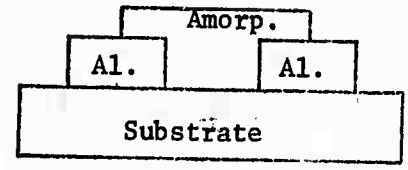

End View

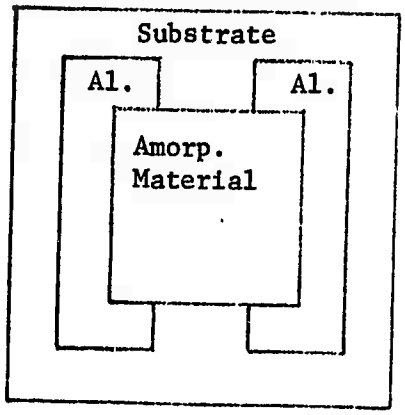

Top View

Figure 3-3: Device Structure Used For TSC Experiment.

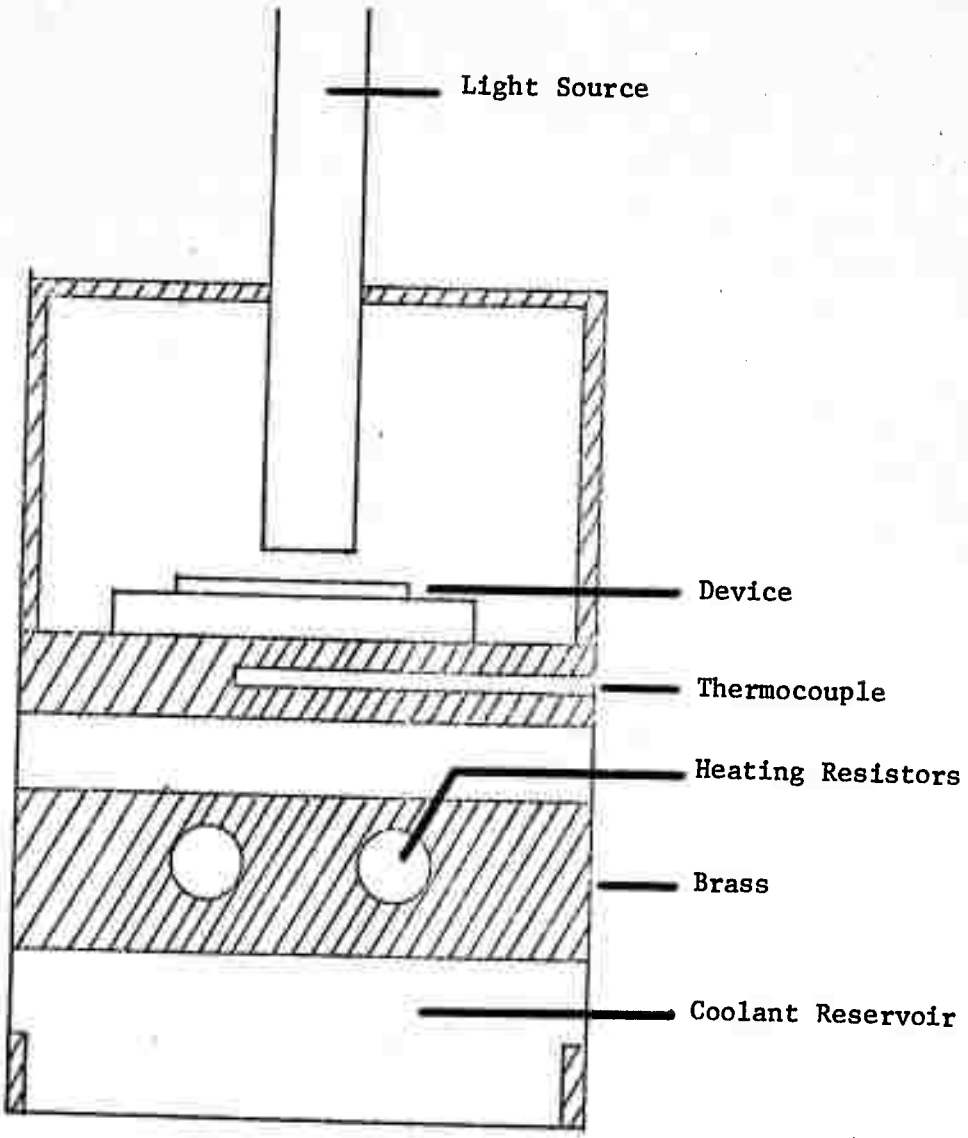

Figure 3-4: Device Holder.

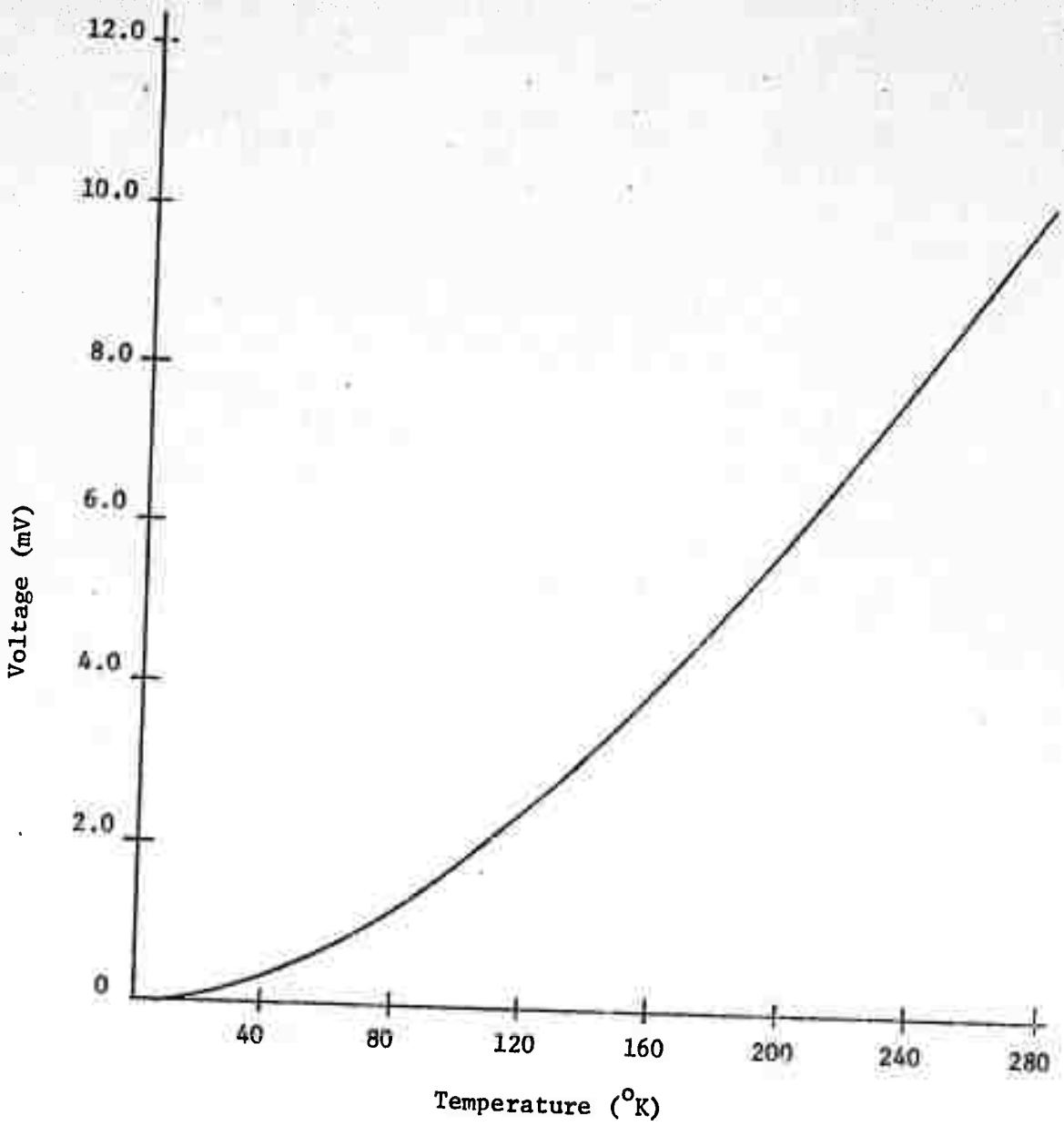

Figure 3-5: Output Curve for Chromel-Constantan Thermocouple (Voltage vs. Temperature). From NBS Report 9712.

3-4.2 Sample Heater

It was determined that a linear heating rate was needed to simiplify the data analysis as much as possible. In order to determine the characteristics of the holder system, a cooling curve was taken as shown in Figure 3-6, and a heating curve was made using a constant input for the heater supply as shown in Figure 3-7. As can be seen from the cooling curve the system has a time constant of approximately 1.3 hours. It may also be noted that a minimum of 6 hours is needed for the cooling system to become stable.

Since resistive heating is proportional to the square of the voltage input, for a constant input voltage one might expect a parabolic heating curve. However, as shown in Figure 3-7, this was not the case since the thermal capacitance of the system completely dominated the heating. For this reason a feedback control system was designed to control the heater input voltage by comparing the system temperature to a predetermined reference voltage. However, this approach was complicated by the fact that the thermocouple output voltage is not linear with temperature as shown in Figure 3-5. The curve in Figure 3-5 suggested the use of a parabolic reference voltage, and the reference was obtained by integrating a constant input voltage twice as shown in Figure 3-8.

Figure 3-8 shows the complete heating circuit. A constant input voltage (V_{in}) is integrated twice by operational amplifier integrators to achieve a slow rising parabolic reference voltage as shown in Figure 3-9. This reference is then compared with the output voltage of the thermocouple amplified by a HP 412 VTVM by a differential amplifier which controls a programmable power supply. The power supply used for heating is a Harrison 6267A programmable D.C. power supply.

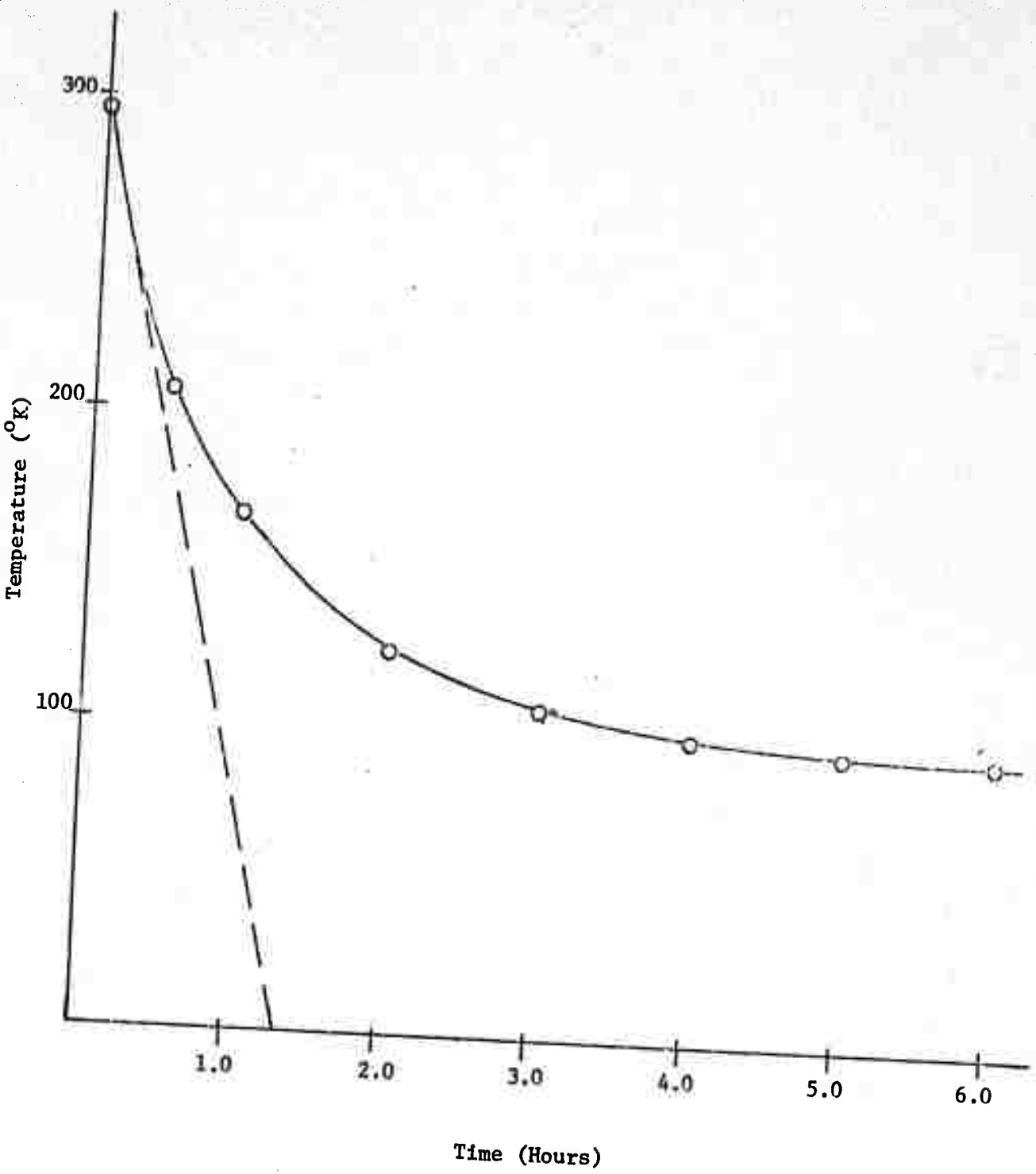

Figure 3-6: System Cooling Curve (Temp. vs. Time).

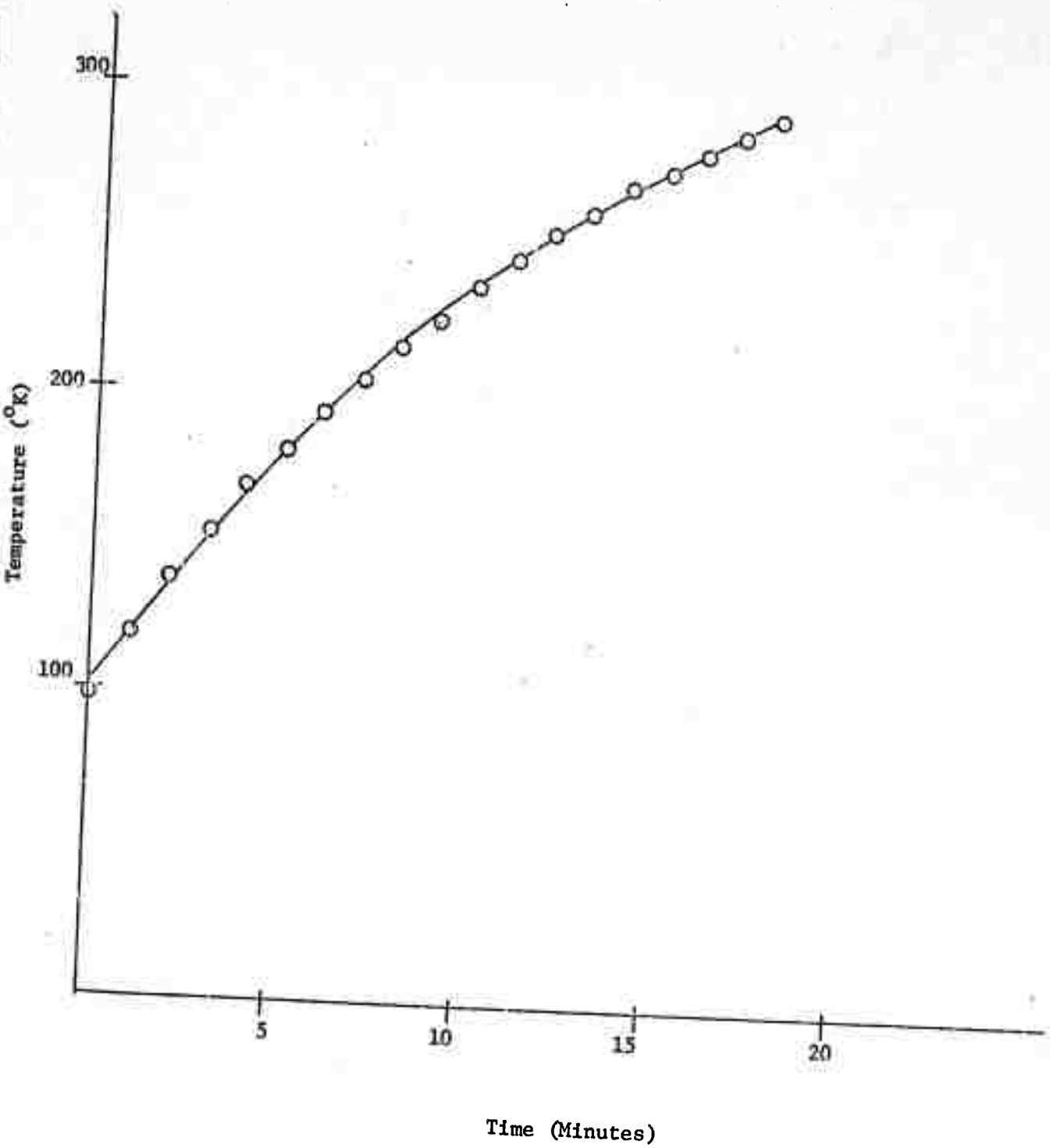

Figure 3-7: System Heating Curve for a Constant Input Voltage (Temp. vs. Time)

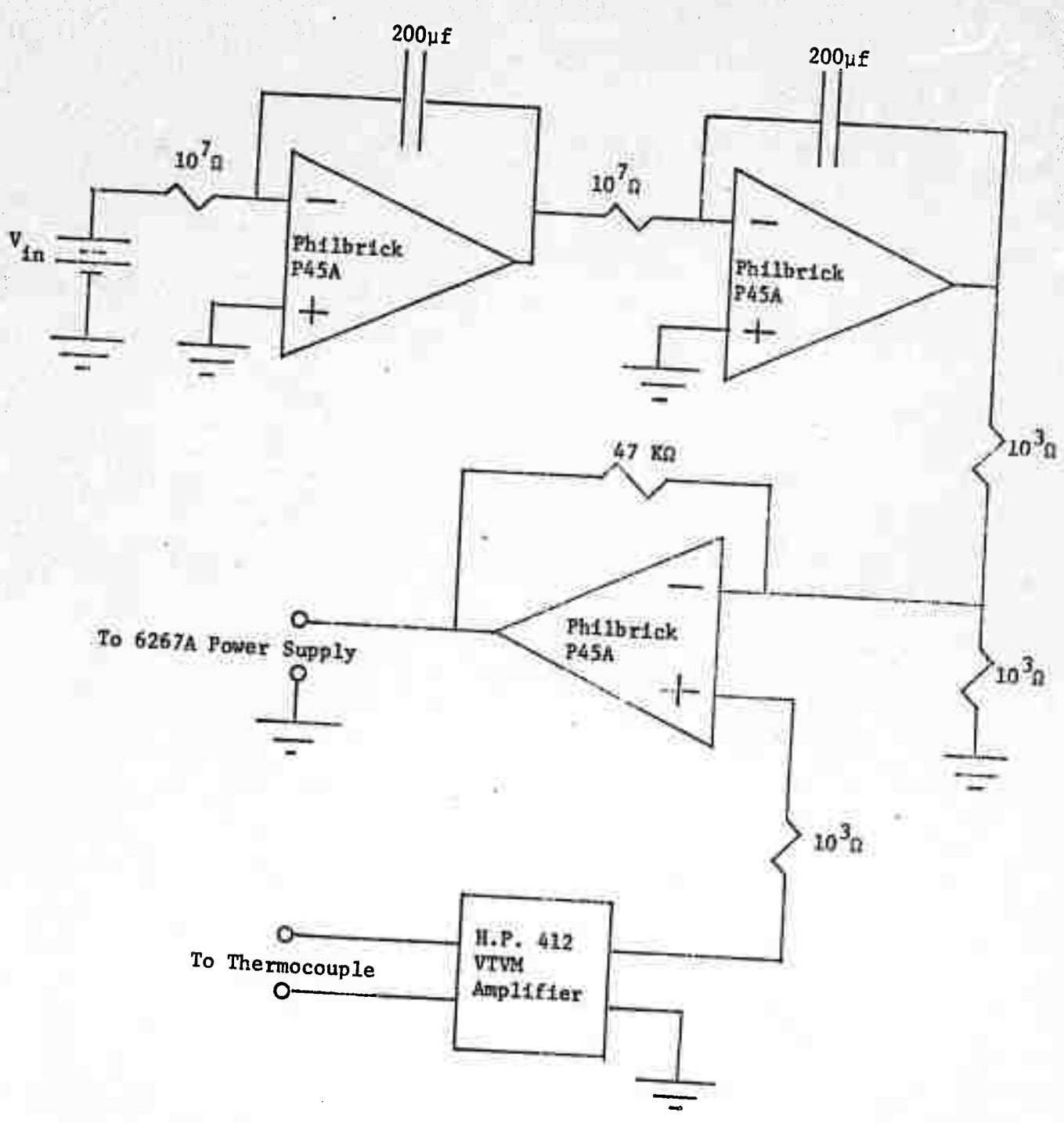

Figure 3-8: System Heating Control Circuit.

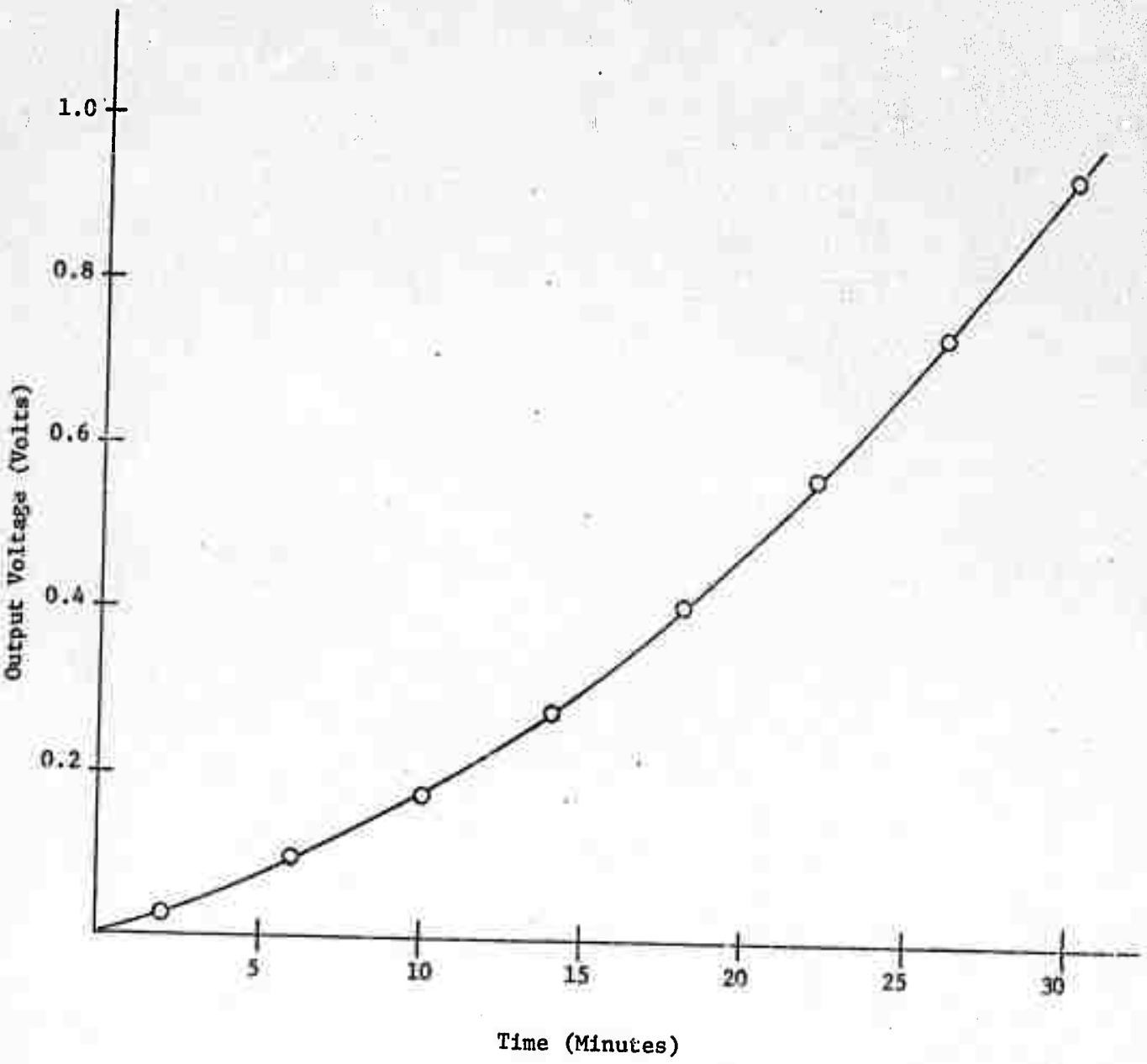

Figure 3-9: Parabolic Reference Voltage. (Voltage vs. Time)

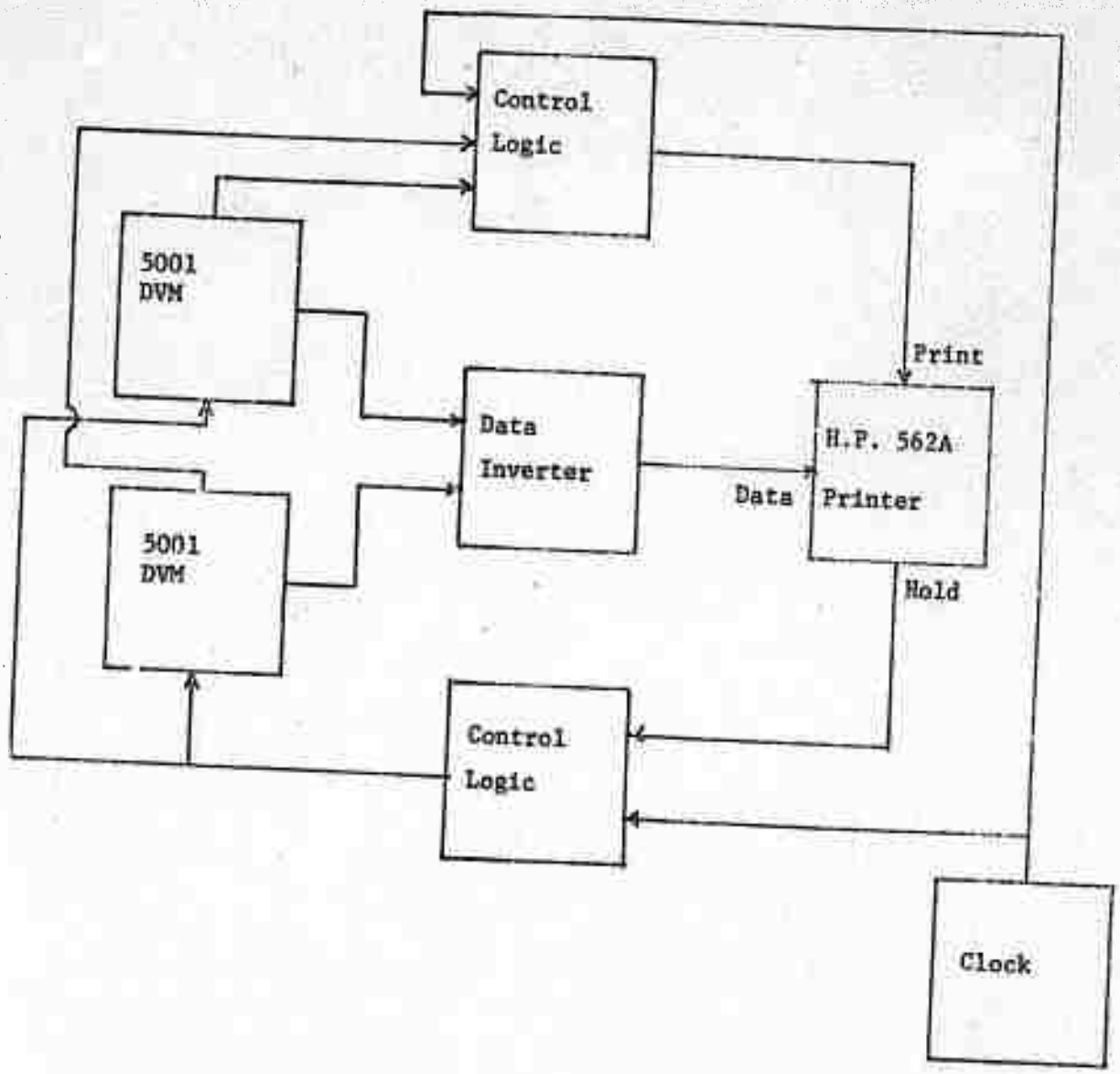

Figure 3-10: Block Diagram of Data Recording System.

3-4.3 Data Recorder

Several methods of recording the output data of the experiment were considered. There are two independent data outputs (temperature and device current) which have to be correlated.

It was then decided to record the data digitally using two E.A.I. 5001 digital voltmeters and an HP 562A printer as shown in Figure 3-10. Figure 3-10 is a block diagram of the circuit used to correlate the meters and control the printer. The printing frequency was arbitrarily chosen to be 0.5 Hz.

The system temperature is recorded at the output of the HP 412. Two representative heating curves using this control system are shown in Figure 3-11.

Initial calibration of the system will be made by comparing results of TSC measurements on known materials such as Al_2O_3 and CdS.

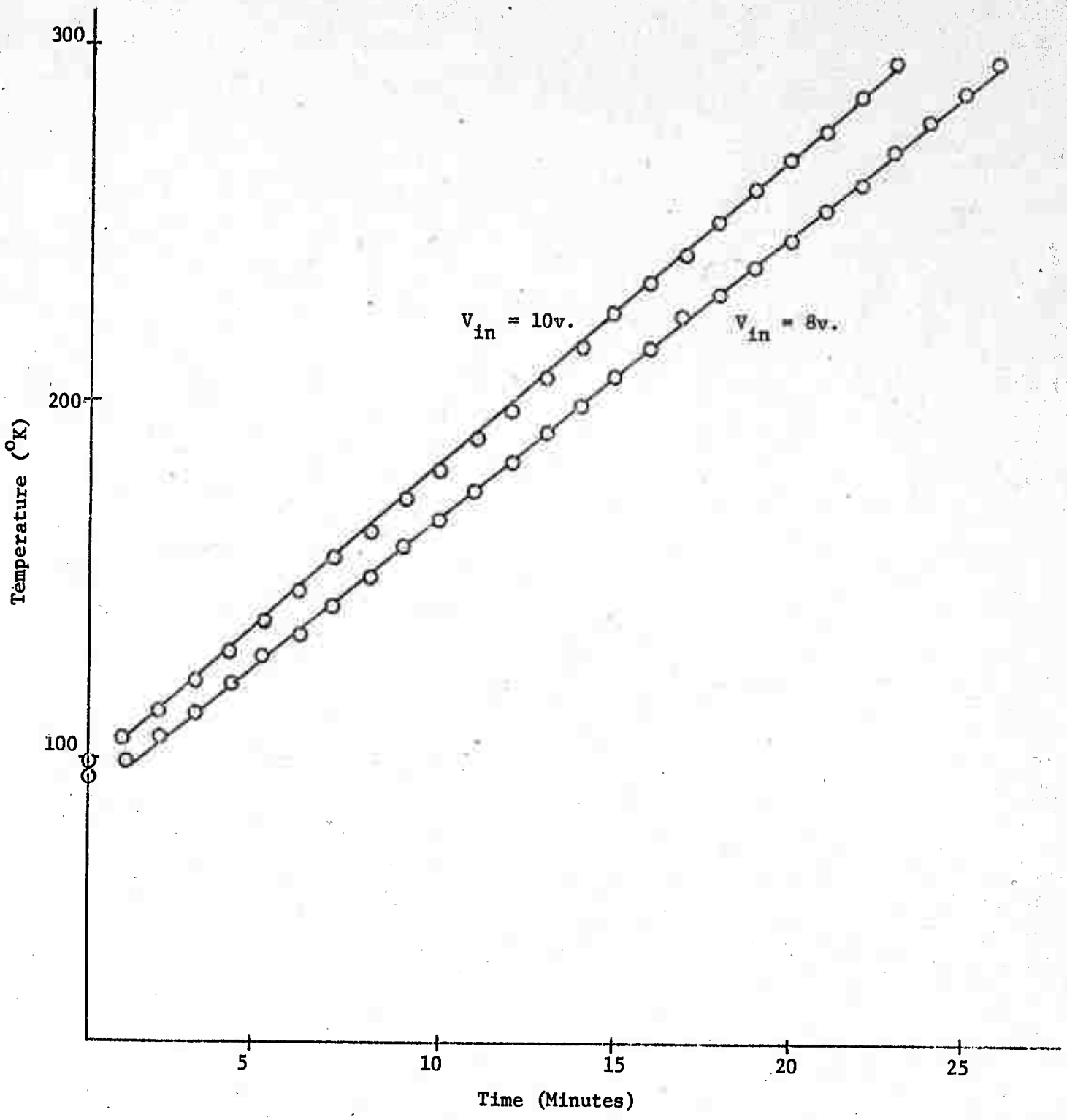

Figure 3-11: System Heating Using the Heater Control System (Temp. vs. Time)

4. Hall Effect in Insulating Solids

4-1 Introduction

The difficulties encountered in making Hall measurements on low mobility solids is directly reflected in the small number of reports of data for amorphous materials. Early work by Kolomiets and Nazarova[33] for Tl_2Se-$As_2(Se,Te)_3$ using AC techniques at room temperature showed Hall mobilities of approximately 10^{-2} $cm^2/(volt\text{-}sec)$ independent of composition. Peck and Dewald[34] used standard DC techniques for the As-Te-I and As-Te-Br systems and found nearly temperature independent mobilities of the order 0.05 $cm^2/(volt\text{-}sec)$. Somewhat contradictory results by Ivkin et al.[35] for the composition Tl_2Se-As_2Te_3 are reported. They found a definite temperature and compositional dependence in the range -30 to 70°C with typical values of the order 0.09 $cm^2/(volt\text{-}sec)$. Hall mobility found by Male[36] for As_2Se_3-0.5 As_2Te_3 and As_2Se_3-2As_2Te_3 are 0.09 $cm^2/(volt\text{-}sec)$ with a slow temperature variation. Most recent measurements by Roilos [37] on the glasses As_2Se_3-xAs_2Te_3 with x = 0.5,1,1.5,2.5, and 3 were reported in the temperature range -10 to 100°C. The Hall coefficient varied exponentially with temperature. The activation energy of the Hall mobility was calculated to lie in the range 0.07 to 0.11 eV with x in the range 0.5 to 3. In all cases reported the sign of the Hall coefficient indicates n-type conduction, in direct conflict of the P-type conduction indicated by thermoelectric measurements.

4-2 Space Charge Limited Currents in an Insulator with Traps

In the study of the Hall effect of insulators, one finds several problems different from those encountered in metals and semiconductors[38]. First, Ohm's law does not apply because the conductivity is not uniform

which implied that the carriers distribution is not uniform. In other words, insulators are affected by space-charge-limited (SCL) current[39,40]. This is a result of the lack of mobile carriers in insulators to conduct current. The small amount of current that does flow through the insulator is caused by carriers which are injected at the electrodes. Thus, the density of carriers is greater at the electrodes than it is in the material. Therefore, the distribution of the carriers, passing from the surface into the material, is affected by the charge of those previously introduced, or they are space-charge-limited.

The second problem encountered is caused by the low-symmetry of most insulators (amorphous materials). The Hall effect, as treated in textbooks, deals with the cubic crystals and not the more complex amorphous materials. Also, a large number of defects are known to exist in amorphous materials, which leads to ionic conduction, and, thus, affects the Hall effect experiment.

A third consideration, is the effect of traps on the Hall experiment. Traps in amorphous materials, caused by impurities and lattice imperfections, are common. These traps effect the number of free carriers available for conduction, and will be shown to reduce the space-charge-limited current in the material.

The effects of various symmetries are dependent upon the type of materials used and a knowledge of any symmetries that may exist. It will be shown that the true J vs V (current density vs voltage) curve is confined within a "triangle" on the log J vs log V plane as shown in Figure 4-1. The "triangle" is bounded below by Ohm's law (J vs V), above by Child's law for solids (J vs V^2), and a trap-filled-limit (TFL) CURVE. For neutral crystals, Ohm's law is valid, that is, $J = en_o\mu v/s$, where

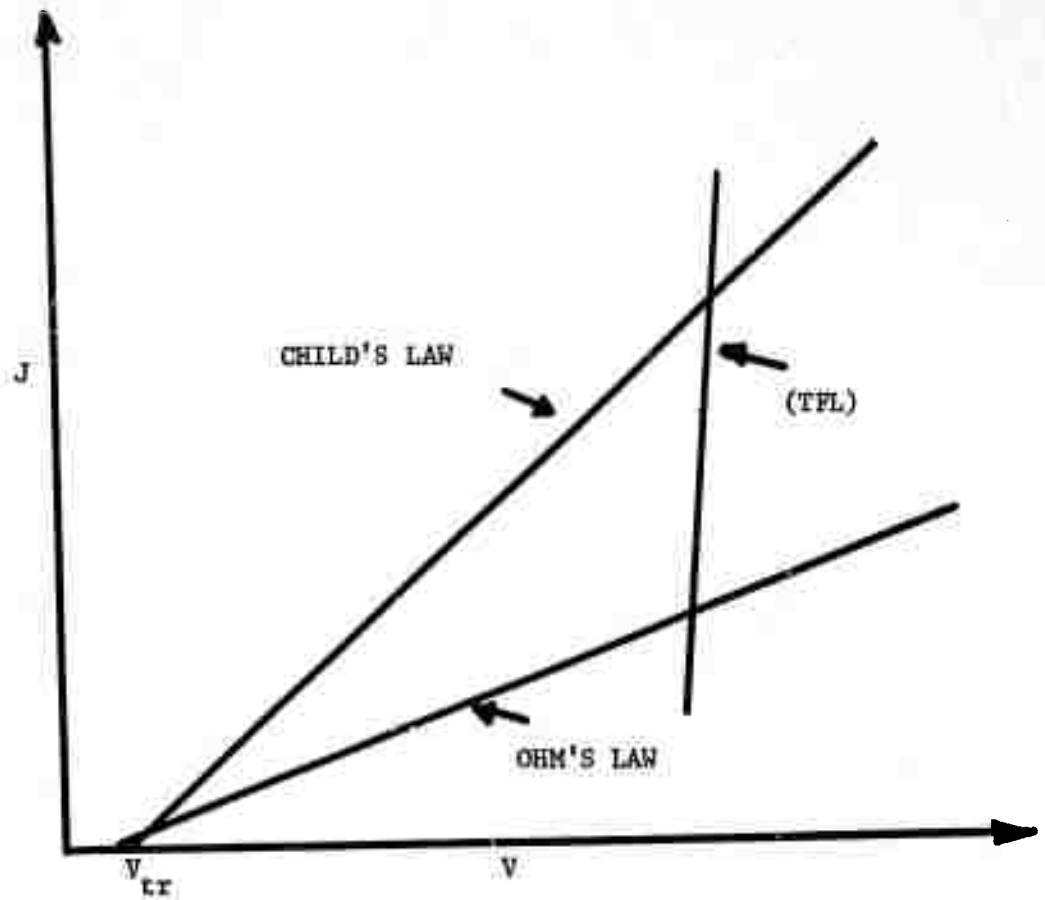

Figure 4-1. Boundaries for Ohm's Law, Child's Law, and TFL

$e \equiv$ charge of carrier,

$n_o \equiv$ thermal equilibrium free carrier density,

$\mu \equiv$ mobility of carriers,

$v \equiv$ voltage applied, and

$s \equiv$ length or thickness of material.

Later it will be shown, that for a trap-free crystal, with negligible diffusion current, Child's law is valid, that is,

$$J = 9/8[\varepsilon\mu v^2/s^3]$$

where ε = Dielectric constant.

When all the traps are filled prior to the application of a voltage, then the trap-filled-limit (TFL) curve is valid.

Since the electrons, at the cathode or emitter, add to the carriers already present, it implies that the true J vs V curve cannot lie below the Ohm's law line. Also, the true curve cannot lie above Child's law line, because Child's law line represents the case where all carriers are in the conduction band. That is, if any carriers are trapped then the curve will lie below Child's law line. For the true (J vs V) curve to lie below the (TFL) curve implies that injected carriers are being immobilized in some other way besides the traps. Since we are not considering any other sink for carriers than the traps, this implies that the true (J vs V) curve is above the (TFL) curve.

Since, in an insulator, we inject the current carriers, and, thus, know the type of carriers, we can assume one-carrier space-charge-limit flow. The current density in a material is the difference between the drift current and the diffusion current. That is,

$$j = ne\mu E - De(dn/dx) \qquad 4\text{-}1$$

where

$n = n(x) \equiv$ number of free carriers at x,

$E = E(x) \equiv$ electric field at x,

$\mu \equiv$ mobility of carrier,

$D \equiv$ diffusion coefficient, and

$e \equiv$ charge of carrier.

Substituting Poisson's equation,

$$dE/dx = ne/\varepsilon \qquad 4\text{-}2$$

into equation 4-1, gives

$$J = \varepsilon\mu E(dE/dx) - \varepsilon D(d^2E/dx^2) \qquad 4\text{-}3$$

where $\varepsilon \equiv$ dielectric constant.

Neglecting the last term, which is permissible if $kT \ll eEs$, one finds

$$E(dE/dx) = J/\varepsilon\mu. \qquad 4\text{-}4$$

The solution to equation 4-4 is

$$E = \sqrt{(2J/\varepsilon\mu)(x + x_o)}. \qquad 4\text{-}5$$

Note that this implies a purely field driven current with no diffusion current. This result is inaccurate near the injecting cathode, where E = 0 and the current is pure diffusion.

The constant of integration x_o of equation 4-5 can be calculated from the boundary condition that at x = 0, $n = N_o$. Where N_o is the electron density at the metal-insulator interface, Therefore, when $n = N_o$,

$$E = J/N_o e\mu \qquad \text{(from equation 4-1)}.$$

Substituting the above equation into equation 4-5 we find

$$x_o = kJ/\mu N_o^2 e^2 \qquad 4\text{-}6$$

The electric potential across the insulator is given by

$$V = \int_0^s E\,dx$$

$$V = \int_0^s 2J/\varepsilon\mu(x + x_o)\,dx, \text{ and}$$

$$V = 2/3\ \sqrt{(2J/\varepsilon\mu}\ ((s + x_o)^{3/2} - x_o^{3/2}).$$

Thus, for $x_o << s$,

$$J = 9/8[\varepsilon\mu V^2/s^3] \qquad 4\text{-}7$$

where s ≡ length of material in x direction.

If the injected carriers density, n_o, caused by thermal energy, then Ohm's law is valid.

$$J = en_o\mu v/s \qquad 4\text{-}8$$

(Note that this is just equation 4-1 with $dn/dx = 0$).

At low voltage, the true curve follows Ohm's, until the voltage increases to the transitive voltage, (V_{tr}) given by setting equation 4-7 and 4-8 equal.

$$en_o\mu V_{tr}/s = 9/8\varepsilon\mu V_{tr}^2/s^3,$$

$$V_{tr} = 8en_o s^2/9\varepsilon \qquad 4\text{-}9$$

When traps are present, the space-charge-limited current is reduced for any given voltage. So, to show the effect traps have on the current, one needs to know the ratio of free carriers to trap carriers, or

$$\theta = n(x)/n_t(x) \qquad 4\text{-}10$$

where $n(x)$ ≡ free carrier density, and

$n_t(x)$ ≡ density of carriers in traps.

By Fermi-Dirac and Boltzmann statistics, one knows that

$$n(x) = N_c \exp\left[\frac{E_f - E_c}{kT}\right] \qquad 4\text{-}11$$

and

$$n_t(x) = \frac{N_t}{1 + \frac{1}{g}\exp\left[\frac{E_t - E_f}{kT}\right]} \qquad 4\text{-}12$$

Where N_c ≡ effective density of states in conduction band,

E_f ≡ Fermi level,

E_c ≡ energy of conduction band,

N_t ≡ trap density, and

g ≡ degeneracy factor for traps. ($g = 2$ in the simpliest case).

Combining equation 4-11 and 4-12 we find

$$n_t(x) = \frac{N_t}{1 + \frac{N}{gN_t}} \qquad 4\text{-}13$$

where $N = N_c \exp\left[\frac{E_t - E_c}{kT}\right]$.

Note, E_f is a function of $n(x)$ and thus is a function of voltage.

Now we shall define shallow traps as being traps located at the least kT above the Fermi level. And, also, shall define deep traps as being at the least kT below the Fermi level. Therefore, from equation 4-13 for shallow traps one finds that

$$1 + \frac{N}{gn(x)} \simeq \frac{N}{gn(x)} \qquad 4\text{-}14$$

and

$$\theta = \frac{n(x)}{n_t(x)} \simeq \frac{N}{gN_t} = \frac{Nc \exp\left[\frac{E_t - E_c}{kT}\right]}{gN_t} \qquad 4\text{-}15$$

Also for deep traps, one notes that

$$1 + \frac{N}{gn(x)} \simeq 1 \qquad 4\text{-}16$$

or

$$n_t(x) \simeq N_t \qquad 4\text{-}17$$

Note, from equation 4-15 that the smaller θ is, the more effective the traps are in reducing the free carrier density. Therefore, a higher voltage is required to produce an injected carrier density greater than the thermal carrier density N_o. Thus, equation 4-7 becomes

$$J = \frac{9}{8}\,\theta\varepsilon\mu\,\frac{V^2}{s^3} \qquad 4\text{-}18$$

and

$$V_{tr} = \frac{8}{9}\,\frac{en_o s^2}{\theta\varepsilon}$$

For deep traps, from equation 4-17, it is shown that all the traps are filled. If all the traps are filled then they cannot be used to immobilize any more carriers from the injected carrier density. Thus, the injected carriers are not reduced by traps and, therefore, the current increases to the trap free space-charge-limit current. Note also, that an increase in voltage, increases the injected carrier density, thus moves the Fermi level

up toward the conduction band, thereby increasing the number of deep traps. When the voltage increases to the trap-filled-limit voltage, all the traps are full, so they cannot keep the current from increasing to the free space-charge-limit current level.

REFERENCES

1) B. T. Kolomiets and V. M. Lyubin, Sov. Phys. - Doklady 4 (1959) 1345.

2) B. T. Kolomiets and V. M. Lyubin, Sov. Phys. - Solid State 2 (1960) 46.

3) B. T. Kolomiets and V. M. Lyubin, Sov. Phys. - Solid State 4 (1962) 291.

4) E. A. Fagen and H. Fritzsche, J. Non-Crystalline Solids 2 (1970) 180.

5) R. Andreichin, J. Non-Crystalline Solids 4 (1970) 73.

6) B. T. Kolomiets, T. F. Mazets, and SH. M. Efendiev, J. Non-Crystalline Solids 4 (1970) 45.

7) G. D. Arndt, W. H. Hartwig, and J. L. Stone, J. Appl. Phys. 39 (1968) 2653.

8) W. H. Hartwig and J. J. Hinds, J. Appl. Phys. 40 (1969) 2020.

9) M. Sucher and J. Fox, Handbook of Microwave Measurements (Interscience Publishers, New York, 1963).

10) J. L. Stone, Ph.D. Dissertation, University of Texas (1968).

11) G. Dresselhaus, A. F. Kip, and C. Kittel, Phys. Rev., 100 (1955) 618.

12) R. E. Michel and B. Rosenblum, Phys. Rev. 128 (1962) 1646.

13) M. H. Cohen, J. Non-Crystalline Solids 2 (1970) 432.

14) A. M. Andriesh and B. T. Kolomiets, Sov. Phys. - Solid State 5 (1963) 1063.

15) . Botila and A. Vancu, Mater. Res. Bull. 5 (1970) 925.

16) B. J. Kolomiets, V. M. Lyubin, and V. L. Averjanov, Mater. Res. Bull. 5 (1970) 655.

17) H. Fritzsche, J. Non-Crystalline Solids 6 (1971) 49.

18) E. A. Davis, Private Communication to J. L. Stone.

19) G. F. J. Garlick and A. F. Gibson, Proc. Phys. Soc. 60 (1948) 574.

20) R. H. Bube, J. Chem. Phys. 23 (1955) 18.

21) W. Hoogenstraaten, Philips Res. Rep. 13 (1958) 515.

22) R. R. Haering and E. A. Adams, Phys. Rev. 117 (1960) 451.

23) P. N. Keating, Proc. Phys. Soc. 78 (1961) 1408.

24) A. Halperin and A. A. Braner, Phys. Rev. 117 (1960) 408.

25) L. F. Grossweiner, J. Appl. Phys. 24 (1953) 1306.

26) C. B. Luschik, Dokl. Akad. Nauk. SSSR, 101 (1955) 641.

27) M.E. Haine and R. E. Carley-Read, Brit. J. Appl. Phys. 1 (1968) 1257.

28) K. H. Nicholas and J. Woods, Brit. J. Appl. Phys. 15 (1964) 783.

29) H. J. Dittfeld and J. Voight, Phys. Status. Sol. 3 (1963) 1941.

30) R. H. Bube, G. A. Dussel, C. T. Ho, and L. D. Miller, J. Appl. Phys. 37 (1966) 21.

31) G. A. Dussel and R. H. Bube, Phys. Rev. 155 (1967) 764.

32) R. H. Bube, Photoconductivity of Solids, John Wiley and Sons, Inc. 1960.

33) B. T. Kolomiets and T. F. Nazarova, Sov. Phys. - Solid State 2 (1960) 369.

34) W. F. Peck, Jr. and J. F. Dewald, J. Electrochem. Soc. 111 (1964) 561.

35) E. B. Ivkin, B. T. Kolomiets, and E. A. Lebedev, Bull. Acad. Sci. USSR Phys. 28 (1964) 1190.

36) J. C. Male, Brit. J. Appl. Phys., 18 (1967) 1543.

37) M. Roilos, J. Non-Crystalline Solids 6 (1971) 5.

38) O. S. Mortensen, R. W. Munn, and D. F. Williams, J. Appl. Phys. 42 (1971) 1192.

39) A. Rose, Phys. Rev. 97 (1955) 1538.

40) M. Lampert, Phys. Rev. 103 (1956) 1648.